Precise PMU-Based Localization and Classification of Short-Circuit Faults in Power Distribution Systems

Denis Sodin, Miha Smolnikar, Urban Rudež, *Member, IEEE*, and Andrej Čampa

***Abstract*—Knowing the exact location of a short-circuit fault in a power distribution system (PDS) is essential for rapid restoration of service to customers and has a direct impact on the operational costs and reliability of the system. In this paper a phasor measurement unit (PMU) based method for fault localization and classification is presented. By introducing the concept of a virtual bus, the exact fault location on the line is determined rather than just a bus closest to the fault. Moreover, after determining the fault location, a generic fault model (GFM) is introduced to classify the type of fault by solving a minimization problem, which also provides fault impedances as a result. These can then be further used to determine if the fault occurred on the lateral instead of the main feeder without using additional PMU at the end of that lateral. The effectiveness of the proposed approach is verified by simulating various fault scenarios in two test systems based on real PDSs using a real-time digital simulator. In addition, a sensitivity analysis of the method is performed for different noise levels in the input parameters to verify its applicability to the real system.**

***Index Terms*—Fault classification, fault localization, phasor measurement unit (PMU).**

I. Introduction

POWER distribution systems (PDSs) are susceptible to various types of faults [1], caused by unpredictable events such as severe weather (sleet, lightning, high winds), tree or animal contact, lack of maintenance, equipment failure, etc. Faults can be either temporary (the fault is successfully cleared by automatic reclosing of the circuit breaker) or permanent. In the first case, an immediate response by the distribution system operator (DSO) is not required, as the fault is self-cleared and the customers are only affected by a power outage for a short period of time. Nevertheless, recurring faults at the same location may indicate poor management of vegetation in a particular part of the network or mechanical problems with equipment, such as aged or damaged insulation, which may be rectified before they escalate to a permanent fault. A permanent fault, on the other hand, always requires a repair crew to be dispatched to the fault location in order to manually clear the fault and restore power supply to customers as quickly as possible. In both cases, precise fault localization is of paramount importance to minimize the downtime of the affected part of the system, mitigate economic losses and improve power quality indices such as system average interruption duration (SAIDI) and customer average interruption duration (CAIDI). As a result, much research has been put into developing new, more efficient methods of fault localization [2]. In the past, these were generally divided into two groups [3]: Travelling wave and impedance-based methods. While travelling wave methods are very accurate in transmission networks, their application in distribution networks becomes very complicated due to the numerous laterals and the resulting reflected waves [4]. In addition, these methods require expensive measurement equipment with high sampling rates capable of detecting wavefronts travelling at near the speed of light. Impedance-based methods [5], on the other hand, rely on calculating the impedance between the substation and the fault. They are therefore simple and inexpensive to implement in real systems, but usually have the problem of providing multiple possible solutions.

With the advent of smart grids and the rapid increase in the use of phasor measurement units (PMUs), a new group of methods has recently emerged. Their main advantage is the use of measurements that are precisely synchronized to a common time reference, which allows direct comparison between measurements from different devices. In addition, the use of phasors (which also contain phase angle information) has been shown to provide more accurate results than simple Root Mean Square (RMS) values [6]. Several algorithms based on synchronized PMU data have already been proposed and are briefly discussed below.

A. Review of Related Work

Table I shows the current state of the art in PMU-based fault localization. The first column of the table lists the leading authors and refers to related research.

In the second column, the methods are divided into five subcategories based on the ascending order of precision with which each method can localize the fault in the network. The first subcategory is labelled *area* and denotes methods that

Manuscript received 14 September 2022; revised 6 February 2023; accepted 16 April 2023. Date of publication 20 April 2023; date of current version 25 September 2023. This work was supported in part by the Slovenian Research Agency under Grants P2-0016 and P2-0356, in part by the EURAMET project FutureGrid II under Grant 17IND06, and in part by the European Commission through the H2020 projects BD4OPEM under Grant 872525, and in part by I-NERGY under Grant 101016508. Paper no. TPWRD-01363-2022. *(Corresponding author: Denis Sodin.)*

Denis Sodin, Miha Smolnikar, and Andrej Čampa are with the Department of Communication Systems, Jožef Stefan Institute, 1000 Ljubljana, Slovenia, and also with the ComSensus d.o.o., 1233 Dob, Slovenia (e-mail: denis.sodin@comsensus.eu; miha.smolnikar@comsensus.eu; andrej.campa@comsensus.eu).

Urban Rudež is with the Faculty of Electrical Engineering, University of Ljubljana, 1000 Ljubljana, Slovenia (e-mail: urban.rudez@fe.uni-lj.si).

Color versions of one or more figures in this article are available at https://doi.org/10.1109/TPWRD.2023.3268767.

Digital Object Identifier 10.1109/TPWRD.2023.3268767

This work is licensed under a Creative Commons Attribution 4.0 License. For more information, see https://creativecommons.org/licenses/by/4.0/

TABLE I
SUMMARY OF THE RELATED WORK

Reference	Fault localization					Hypothesis testing	Fault classification		PMU location	Evaluation tool
	Area	Line	Bus	Exact position	Non-monitored laterals		Fault type	Fault impedance		
Jamei, *et al.* [7]	✓					Yes	×	×	Optimized	OpenDSS
Ardakanian, *et al.* [8]	✓					No	×	×	Every bus	OpenDSS
Biswal, *et al.* [9]	✓					No	×	×	Optimized	PLSF
Conte, *et al.* [10]	✓					No	✓	×	Optimized	DigSil
Ahmed, *et al.* [11]	✓					No	✓	×	Optimized	RTDS & Opal RT
Pignati, *et al.* [12]		✓				Yes	✓	×	Every bus	Opal RT
Li, *et al.* [13]		✓				No	×	×	Optimized	Matlab
Gholami, *et al.* [14]		✓	✓			No	×	×	Optimized	OpenDSS
Pereira, *et al.* [15]			✓			Yes	REQ	×	Optimized	ATP
Majidi, *et al.* [16]			✓			Yes	×	×	Optimized	DigSil
Usman, *et al.* [17]			✓			Yes	×	×	Optimized	Opal RT
Liu, *et al.* [18]			✓			No	×	×	Every bus	Matlab
Farajollahi, *et al.* [19]			✓			No	×	×	Optimized	Matlab
Cavalcante, *et al.* [20]				✓		Yes	×	×	Optimized	ATP
Cui, *et al.* [21]				✓		No	×	×	Every bus	Opal RT
Khaleghi, *et al.* [22]				✓		No	✓	✓	Optimized	EMTP-RV
Lotfifard, *et al.* [23]				✓	✓	Yes	REQ	×	Optimized	ATP
Proposed				✓	✓	No	✓	✓	Optimized	RTDS

are only able to determine a large area or cluster of buses as potential fault candidates [7], [8], [9], [10], [11]. The next two subcategories, *line* and *bus*, can locate the fault with better but comparable precision. As the name implies, the methods in the line subcategory [12], [13], [14] return the faulty line as a result. However, they do not tell anything about the exact position on the line, so a particular line still needs to be inspected manually to pinpoint the fault. Bus methods [14], [15], [16], [17], [18], [19], on the other hand, point to the bus closest to the fault and therefore give perfect results for faults that occur on buses. However, if the fault occurs on the line instead, lines connected to the identified faulty bus must still be inspected manually. The fourth subcategory, [20], [21], [22], [23], called *exact location*, provides even more accurate results, as the methods in this subcategory are able to precisely pinpoint the location of the fault, regardless of whether the fault occurs in one of the buses or somewhere on the line. However, even for most of these methods in the relevant literature, this is only true if the fault occurs on a line that is monitored from both ends. This means that all faults on lateral lines that are not monitored are still referred to as if they occurred on the bus from which the lateral line originates. For this reason, we introduce another subcategory in the table, which contains methods that can also pinpoint faults on *non-monitored laterals*.

Another benchmark for comparing methods in this paper is whether the method is able to determine the location of fault without the use of simulations. Methods that collect and examine data from multiple measurement devices throughout the PDS often operate on the basis of a hypothetical placement of faults at different locations and by varying the fault impedances at that location. The corresponding state (power flow) is then calculated using power system simulation tools for each change in fault location or fault impedance. Finally, the simulation results are compared with field measurements to test each hypothesis, and the scenario with the closest similarity is announced as the solution to the problem. Since such an approach can be very computationally intensive, we indicate in the third column of the table whether or not each of the methods is based on *hypothesis testing*.

In the fourth column of the table, we look at the ability of the methods to classify faults. Fault classification can either be coarse, i.e., it determines only the type of fault, or it can also involve the computation of fault impedances. In this paper, we consider three different options. The methods labelled ✓ provide the classification of the fault, the methods labelled × do not, and the methods labelled REQ require that the type of fault is known in advance in order to perform fault localization.

The precision of fault localization method is often directly related to the number of PMUs used and consequently to the cost of implementing the method in a real environment. Compared to transmission networks, distribution networks consist of many more buses, so installing a PMU in each of these buses may not be financially feasible. For this reason, PMU placement optimization is often considered. The fifth column of the table indicates whether the method assumes that each bus is equipped with the PMU or whether the method considers PMU placement optimization.

The last column of the table does not refer to the performance of the fault localization method, but simply indicates which tool the authors used to test their proposed approach in the laboratory.

B. Paper Contributions

This paper presents a methodology for improved fault localization and classification. The approach is inspired by the previous work in [19], where the bus closest to the fault is determined as faulted. To increase accuracy, a full π model of the lines that includes capacitance (shunt admittance) is used

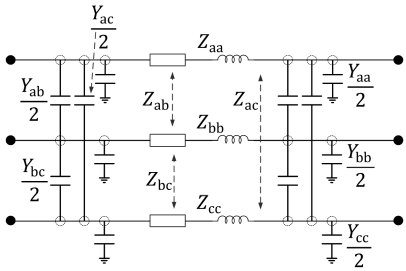

Fig. 1. Complete three-phase π-segment representation of a line.

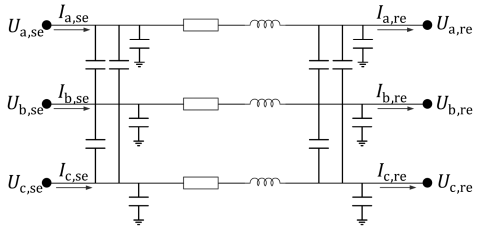

Fig. 2. Voltages and currents in sending and recieving ends of the π-segment.

instead of the simplified serial impedance model. This was done because it was shown in [24] that the capacitive effect on fault localization in distribution networks is not negligible. The goal of this work is to improve the localization capability of the existing method by also investigating faults on lines (between buses) and faults on lateral lines that are not covered by PMUs. Moreover, we intuitively extend the localization functionality by adding a completely new feature, the fault classifier. The contributions of the paper can be listed as follows.

- Improved fault localization algorithm capable of determining the exact location on the line rather than just the bus closest to the fault.
- Introduction of a generic fault model (GFM) capable of identifying the faulted phases as well as determining fault impedances.
- Novel approach of localizing faults on the laterals that are not being monitored.

II. Mathematical Background of the π-Segment Model of a Line

Consider a three-phase distribution line represented by its complete π-segment model. Using the notations in Fig. 1, we can define the impedance matrix $\mathbf{Z}$ and the admittance matrix $\mathbf{Y}$ of this segment as follows:

$$\mathbf{Z} = \begin{bmatrix} Z_{aa} & Z_{ab} & Z_{ac} \\ Z_{ba} & Z_{bb} & Z_{bc} \\ Z_{ca} & Z_{cb} & Z_{cc} \end{bmatrix}, \quad \mathbf{Y} = \begin{bmatrix} Y_{aa} & Y_{ab} & Y_{ac} \\ Y_{ba} & Y_{bb} & Y_{bc} \\ Y_{ca} & Y_{cb} & Y_{cc} \end{bmatrix}. \tag{1}$$

Z_{aa}, Z_{bb}, Z_{cc} are the serial impedances of the phases, Y_{aa}, Y_{bb}, Y_{cc} are the shunt capacitances of the phases, Z_{ab}, Z_{bc}, Z_{ac}, Z_{ba}, Z_{cb}, Z_{ca} are the phase to phase impedances, and Y_{ab}, Y_{bc}, Y_{ac}, Y_{ba}, Y_{cb}, Y_{ca} are the phase to phase admittances.

Note that no simplification is made in terms of symmetry between phases to account for unbalanced conditions in distribution systems such as non-transposed lines and parts with one or two phases. The voltages and currents over the π-segment at the receiving and sending ends (indices re and se, respectively) are calculated as follows:

$$\begin{bmatrix} \mathbf{U}_{abc,re} \\ \mathbf{I}_{abc,re} \end{bmatrix} = \mathbf{\Pi}^{-1} \cdot \begin{bmatrix} \mathbf{U}_{abc,se} \\ \mathbf{I}_{abc,se} \end{bmatrix} = \begin{bmatrix} \mathbf{D} & -\mathbf{B} \\ -\mathbf{C} & \mathbf{A} \end{bmatrix} \cdot \begin{bmatrix} \mathbf{U}_{abc,se} \\ \mathbf{I}_{abc,se} \end{bmatrix} \tag{2}$$

for the forward calculation, and

$$\begin{bmatrix} \mathbf{U}_{abc,se} \\ \mathbf{I}_{abc,se} \end{bmatrix} = \mathbf{\Pi} \cdot \begin{bmatrix} \mathbf{U}_{abc,re} \\ \mathbf{I}_{abc,re} \end{bmatrix} = \begin{bmatrix} \mathbf{A} & \mathbf{B} \\ \mathbf{C} & \mathbf{D} \end{bmatrix} \cdot \begin{bmatrix} \mathbf{U}_{abc,re} \\ \mathbf{I}_{abc,re} \end{bmatrix} \tag{3}$$

for the backward calculation. The π-segment parameter matrices $\mathbf{A}$, $\mathbf{B}$, $\mathbf{C}$, $\mathbf{D}$ are defined as follows:

$$\mathbf{A} = \mathbf{D} = \mathbb{I} + \frac{1}{2}\mathbf{Z} \cdot \mathbf{Y},$$

$$\mathbf{B} = \mathbf{Z},$$

$$\mathbf{C} = \mathbf{Y} + \frac{1}{4}\mathbf{Y} \cdot \mathbf{Z} \cdot \mathbf{Y},$$

and $\mathbb{I}$ is a 3×3 unitary matrix. According to Fig. 2, $\mathbf{U}_{abc,re}$, $\mathbf{I}_{abc,re}$ are the voltages and currents of all three phases at the receiving end of π-segment:

$$\mathbf{U}_{abc,re} = \begin{bmatrix} U_{a,re} \\ U_{b,re} \\ U_{c,re} \end{bmatrix}, \quad \mathbf{I}_{abc,re} = \begin{bmatrix} I_{a,re} \\ I_{b,re} \\ I_{c,re} \end{bmatrix}.$$

Similarly, $\mathbf{U}_{abc,se}$, $\mathbf{I}_{abc,se}$ are the voltages and currents at the sending end of the π-segment:

$$\mathbf{U}_{abc,se} = \begin{bmatrix} U_{a,se} \\ U_{b,se} \\ U_{c,se} \end{bmatrix}, \quad \mathbf{I}_{abc,se} = \begin{bmatrix} I_{a,se} \\ I_{b,se} \\ I_{c,se} \end{bmatrix}.$$

For simplicity, we will omit the subscript abc from now on, keeping in mind that all voltages and currents are three-phase values. Instead, we will use the subscript i to denote the bus whose values we are observing. To be consistent with the labels used in [19], we will also use the superscripts f and b to indicate when we are dealing with forward or backward direction of calculation. The voltages and currents of the i-th bus are then calculated in the forward and backward directions as follows:

$$\begin{bmatrix} \mathbf{U}_i^f \\ \mathbf{I}_i^f \end{bmatrix} = \mathbf{\Pi}_{i-1}^{-1} \cdot \begin{bmatrix} \mathbf{U}_{i-1}^f \\ \mathbf{I}_{i-1}^f \end{bmatrix}, \quad \begin{bmatrix} \mathbf{U}_i^b \\ \mathbf{I}_i^b \end{bmatrix} = \mathbf{\Pi}_i \cdot \begin{bmatrix} \mathbf{U}_{i+1}^b \\ \mathbf{I}_{i+1}^b \end{bmatrix}. \tag{4}$$

III. Methodology

In this section, four segments of the proposed fault localization and classification methodology are explained in detail (Sections III-A through III-D). Finally, a complete flowchart of the method is presented in Section III-E.

A. Existing Fault Localization Method

In the study [19], the voltage and current variations recorded by the PMUs before and during (superscripts pre and post, respectively) the fault were used, so that

$$\Delta \mathbf{U}_{\mathrm{i}} = \mathbf{U}_{\mathrm{i}}^{\mathrm{post}} - \mathbf{U}_{\mathrm{i}}^{\mathrm{pre}}, \tag{5}$$

$$\Delta \mathbf{I}_{\mathrm{i}} = \mathbf{I}_{\mathrm{i}}^{\mathrm{post}} - \mathbf{I}_{\mathrm{i}}^{\mathrm{pre}}. \tag{6}$$

To determine the fault location, the voltage and current variations for the forward direction (from the beginning to the end of the feeder) were calculated as follows:

$$\Delta \mathbf{U}_{\mathrm{i}}^{\mathrm{f}} = \Delta \mathbf{U}_{\mathrm{i-1}}^{\mathrm{f}} - \mathbf{Z}_{\mathrm{i-1}} \cdot \Delta \mathbf{I}_{\mathrm{i-1}}^{\mathrm{f}}, \tag{7}$$

$$\Delta \mathbf{I}_{\mathrm{i}}^{\mathrm{f}} = \Delta \mathbf{I}_{\mathrm{i-1}}^{\mathrm{f}} - \mathbf{Y}_{\mathrm{i}}^{\mathrm{lat}} \cdot \Delta \mathbf{U}_{\mathrm{i}}^{\mathrm{f}}, \tag{8}$$

where $\mathbf{Z}_{\mathrm{i}}$ is the simplified serial impedance model of i-th line and $\mathbf{Y}_{\mathrm{i}}^{\mathrm{lat}}$ is the equivalent admittance of lateral i. Similarly, for the calculation in backward direction (from the end to the beginning of feeder), the following equations were used:

$$\Delta \mathbf{U}_{\mathrm{i}}^{\mathrm{b}} = \Delta \mathbf{U}_{\mathrm{i+1}}^{\mathrm{b}} + \mathbf{Z}_{\mathrm{i}} \cdot \Delta \mathbf{I}_{\mathrm{i+1}}^{\mathrm{b}}, \tag{9}$$

$$\Delta \mathbf{I}_{\mathrm{i}}^{\mathrm{b}} = \Delta \mathbf{I}_{\mathrm{i+1}}^{\mathrm{b}} + \mathbf{Y}_{\mathrm{i}}^{\mathrm{lat}} \cdot \Delta \mathbf{U}_{\mathrm{i}}^{\mathrm{b}}. \tag{10}$$

Finally, the voltage discrepancy from both calculations for all buses was defined as follows:

$$\Phi_{\mathrm{i}} = |\Delta \mathbf{U}_{\mathrm{i}}^{\mathrm{f}} - \Delta \mathbf{U}_{\mathrm{i}}^{\mathrm{b}}|, \tag{11}$$

and the bus with the minimum value of Φ was considered as the fault location. In our approach, modified equations are used to account for the complete π-model of the lines, i.e.:

$$\begin{bmatrix} \Delta \mathbf{U}_{\mathrm{i}}^{\mathrm{f}} \\ \Delta \mathbf{I}_{\mathrm{i}}^{\mathrm{f}} \end{bmatrix} = \mathbf{\Pi}_{\mathrm{i-1}}^{-1} \cdot \begin{bmatrix} \Delta \mathbf{U}_{\mathrm{i-1}}^{\mathrm{f}} \\ \Delta \mathbf{I}_{\mathrm{i-1}}^{\mathrm{f}} \end{bmatrix} - \begin{bmatrix} 0 \\ \mathbf{Y}_{\mathrm{i}}^{\mathrm{lat}} \cdot \Delta \mathbf{U}_{\mathrm{i}}^{\mathrm{f}} \end{bmatrix} \tag{12}$$

for the forward direction, and

$$\begin{bmatrix} \Delta \mathbf{U}_{\mathrm{i}}^{\mathrm{b}} \\ \Delta \mathbf{I}_{\mathrm{i}}^{\mathrm{b}} \end{bmatrix} = \mathbf{\Pi}_{\mathrm{i}} \cdot \begin{bmatrix} \Delta \mathbf{U}_{\mathrm{i+1}}^{\mathrm{b}} \\ \Delta \mathbf{I}_{\mathrm{i+1}}^{\mathrm{b}} \end{bmatrix} + \begin{bmatrix} 0 \\ \mathbf{Y}_{\mathrm{i}}^{\mathrm{lat}} \cdot \Delta \mathbf{U}_{\mathrm{i}}^{\mathrm{b}} \end{bmatrix} \tag{13}$$

for the backward direction, but the basic idea of determining the bus with the minimum value of Φ remains.

Two important remarks should be made at this point. First, the existing method did not consider faults outside the buses. That is, if a fault occurred somewhere on the line between two buses, only the bus closest to the fault was determined, not its exact location as well. Such an approach may be appropriate for urban areas where buses are not far apart, but it may be inadequate for rural areas where lines are much longer. Another important aspect of [19] is the concept of minimum spanning tree (MST), which is the path connecting all PMUs in the network. Consider the 16-bus system shown in Fig. 3 and two PMUs installed on buses 1 and 14. The MST of this configuration covers all buses on the main feeder between the PMUs, i.e., buses 1 to 14, but not the laterals stemming from them (in this case, lateral with buses 15 and 16). Since the existing method can only determine MST buses as faulty, faults on the laterals that are not part of the MST are seen as if they occurred instead in the MST bus from which the lateral originates. One way to solve this problem is to install additional PMUs and increase the number of MST

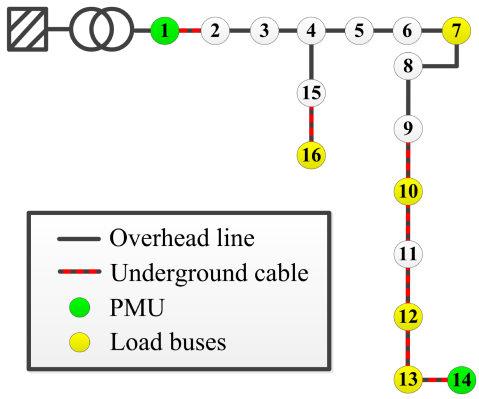

Fig. 3. Single-line diagram of 16-bus MV distribution network.

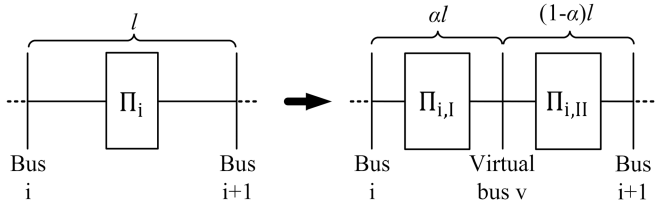

Fig. 4. Splitting the line into two parts and introduction of a virtual bus.

buses. For example, if you install a PMU in bus 16, buses 15 and 16 also become MST buses and can be designated as fault locations. However, installing additional PMU at the end of each lateral and turning every bus in the network into an MST bus for the sole purpose of fault localization would be difficult to justify financially. Therefore, the authors of [19] suggest that MST should be extended strategically; for long lateral lines that include many buses. In contrast, we will show later in this paper (Section III-D) that fault localization is also possible for the lines that are not part of MST without additional PMUs. If they are part of first-degree laterals, i.e. laterals that do not further split into additional branches, the proposed extension provides a unique solution, otherwise one obtains a potential fault location on each of the sublaterals. In this way, an additional layer of the network becomes observable without additional investment. First, however, we present a method for locating a fault on the line between two MST buses.

B. Introduction of the Virtual Bus and Fault Localization on the Lines

From the previous subsection, it is clear that the fault location in [19] is determined to be the MST bus with the minimum value of the voltage discrepancy. However, since the term bus refers to a part of the grid involving either a load / source, a lateral line, or a change in cable type, rather than any point on the line, the exact location of the fault cannot be determined. This deficiency can be efficiently addressed by introducing a virtual bus between two actual MST buses (a bus closest to the fault, determined in the previous step, and an adjacent bus). Imagine that a line between two buses is virtually divided into two parts, one of length αl and the other of length $(1-\alpha)l$, as shown in Fig. 4, where α is a fraction of the total line length l, i.e., $\alpha \in [0, 1]$.

Evidently, the variables **A**, **B**, **C**, **D** must be recalculated for each of the newly introduced π-segments to account for their corresponding length, and can be expressed as follows:

$$\mathbf{A}_{\mathrm{I}} = \mathbf{D}_{\mathrm{I}} = \mathbb{I} + \frac{1}{2}\mathbf{Z}\cdot\mathbf{Y}\alpha^2,$$

$$\mathbf{B}_{\mathrm{I}} = \mathbf{Z}\alpha,$$

$$\mathbf{C}_{\mathrm{I}} = \mathbf{Y}\alpha + \frac{1}{4}\mathbf{Y}\cdot\mathbf{Z}\cdot\mathbf{Y}\alpha^3,$$

for the first π-segment and

$$\mathbf{A}_{\mathrm{II}} = \mathbf{D}_{\mathrm{II}} = \mathbb{I} + \frac{1}{2}\mathbf{Z}\cdot\mathbf{Y}(1-\alpha)^2,$$

$$\mathbf{B}_{\mathrm{II}} = \mathbf{Z}(1-\alpha),$$

$$\mathbf{C}_{\mathrm{II}} = \mathbf{Y}(1-\alpha) + \frac{1}{4}\mathbf{Y}\cdot\mathbf{Z}\cdot\mathbf{Y}(1-\alpha)^3,$$

for the second π-segment. Now, the calculation of the voltages of the virtual bus v in the forward and backward directions is possible, similar to the (2) and (3) as follows:

$$\begin{bmatrix}\Delta\mathbf{U}^{\mathrm{f}}_{\mathrm{v}}(\alpha)\\ \Delta\mathbf{I}^{\mathrm{f}}_{\mathrm{v}}(\alpha)\end{bmatrix} = \mathbf{\Pi}^{-1}_{\mathrm{i,I}}\cdot\begin{bmatrix}\Delta\mathbf{U}^{\mathrm{f}}_{\mathrm{i}}\\ \Delta\mathbf{I}^{\mathrm{f}}_{\mathrm{i}}\end{bmatrix} = \begin{bmatrix}\mathbf{D}_{\mathrm{i,I}} & -\mathbf{B}_{\mathrm{i,I}}\\ -\mathbf{C}_{\mathrm{i,I}} & \mathbf{A}_{\mathrm{i,I}}\end{bmatrix}\cdot\begin{bmatrix}\Delta\mathbf{U}^{\mathrm{f}}_{\mathrm{i}}\\ \Delta\mathbf{I}^{\mathrm{f}}_{\mathrm{i}}\end{bmatrix}, \tag{14}$$

$$\begin{bmatrix}\Delta\mathbf{U}^{\mathrm{b}}_{\mathrm{v}}(\alpha)\\ \Delta\mathbf{I}^{\mathrm{b}}_{\mathrm{v}}(\alpha)\end{bmatrix} = \mathbf{\Pi}_{\mathrm{i,II}}\cdot\begin{bmatrix}\Delta\mathbf{U}^{\mathrm{b}}_{\mathrm{i+1}}\\ \Delta\mathbf{I}^{\mathrm{b}}_{\mathrm{i+1}}\end{bmatrix} = \begin{bmatrix}\mathbf{A}_{\mathrm{i,II}} & \mathbf{B}_{\mathrm{i,II}}\\ \mathbf{C}_{\mathrm{i,II}} & \mathbf{D}_{\mathrm{i,II}}\end{bmatrix}\cdot\begin{bmatrix}\Delta\mathbf{U}^{\mathrm{b}}_{\mathrm{i+1}}\\ \Delta\mathbf{I}^{\mathrm{b}}_{\mathrm{i+1}}\end{bmatrix}. \tag{15}$$

Note, that the computation of the voltages and currents for both forward and backward directions now depends on the variable α, consequently the voltage discrepancy also becomes a function of the variable α, i.e.:

$$\Phi(\alpha) = |\Delta\mathbf{U}^{\mathrm{f}}_{\mathrm{v}}(\alpha) - \Delta\mathbf{U}^{\mathrm{b}}_{\mathrm{v}}(\alpha)|. \tag{16}$$

By changing the position of the bus v from the beginning to the end of the line, the exact fault location on the line can be determined; again, by finding the location with minimal voltage discrepancy. Finding a minimum can be accomplished either by a minimization process or by a simple brute force method of changing the location incrementally by changing the value of the variable α from 0 to 1. In both cases, the desired accuracy can be achieved by setting the termination condition, e.g., the location of the faulted bus is determined within ‰ of the total line length. Of course, this condition can be adjusted and may vary depending on the line lengths considered.

C. Introduction of Generic Fault Model in Faulted Bus and Classification of Fault by Optimization Procedure

Once the fault location is determined, whether the actual physical MST bus or the virtual bus somewhere on the MST line, the fault impedances can be calculated by exploiting the fact that the voltage discrepancy of each bus should converge to 0 if the fault currents are properly accounted for in the equations (note that the voltage discrepancy between forward and backward calculations in each bus is a direct result of the (12) and (13) being an incomplete representation of the fault location, i.e., the fault currents are not included in the equations of the faulted bus). To address this deficiency, a GFM containing all possible combinations of fault types, as shown in Fig. 5, is included in the bus k determined to be faulty in the previous two subsections. According to the figure, the vector of fault currents $\mathbf{I}^{\mathrm{w}}_{\mathrm{fault}}$, where w indicates the direction of the computation, can then be expressed in an expanded form as:

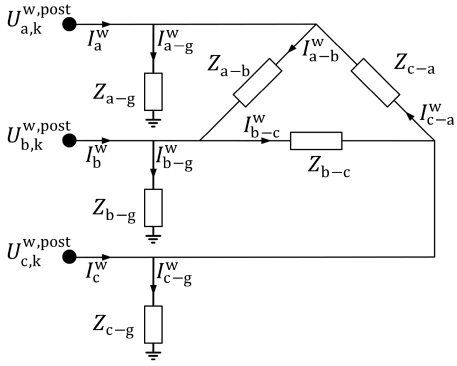

Fig. 5. GFM of possible fault combinations.

$$\mathbf{I}^{\mathrm{w}}_{\mathrm{fault}} = \begin{bmatrix}I^{\mathrm{w}}_{\mathrm{a}}\\ I^{\mathrm{w}}_{\mathrm{b}}\\ I^{\mathrm{w}}_{\mathrm{c}}\end{bmatrix} = \begin{bmatrix}I^{\mathrm{w}}_{\mathrm{a\text{-}g}} + I^{\mathrm{w}}_{\mathrm{a\text{-}b}} - I^{\mathrm{w}}_{\mathrm{c\text{-}a}}\\ I^{\mathrm{w}}_{\mathrm{b\text{-}g}} + I^{\mathrm{w}}_{\mathrm{b\text{-}c}} - I^{\mathrm{w}}_{\mathrm{a\text{-}b}}\\ I^{\mathrm{w}}_{\mathrm{c\text{-}g}} + I^{\mathrm{w}}_{\mathrm{c\text{-}a}} - I^{\mathrm{w}}_{\mathrm{b\text{-}c}}\end{bmatrix}, \tag{17}$$

where each of the contributing currents is calculated as follows:

$$I^{\mathrm{w}}_{\mathrm{x\text{-}g}} = \frac{U^{\mathrm{w,post}}_{\mathrm{x,k}}}{Z_{\mathrm{x\text{-}g}}}, \qquad \mathrm{x}\in\{\mathrm{a,b,c}\}\wedge\mathrm{w}\in\{\mathrm{f,b}\}, \tag{18}$$

$$I^{\mathrm{w}}_{\mathrm{x\text{-}y}} = \frac{U^{\mathrm{w,post}}_{\mathrm{y,k}} - U^{\mathrm{w,post}}_{\mathrm{x,k}}}{Z_{\mathrm{x\text{-}y}}}, \qquad \mathrm{x,y}\in\{\mathrm{a,b,c}\}\wedge\mathrm{x}\neq\mathrm{y}. \tag{19}$$

Here $U^{\mathrm{w,post}}_{\mathrm{x,k}}$ and $U^{\mathrm{w,post}}_{\mathrm{y,k}}$ are voltages of phases x and y in bus k during the fault, $Z_{\mathrm{x\text{-}g}}$ and $I^{\mathrm{w}}_{\mathrm{x\text{-}g}}$ are the fault impedances and fault currents between phase x and ground, and $Z_{\mathrm{x\text{-}y}}$ and $I^{\mathrm{w}}_{\mathrm{x\text{-}y}}$ are the fault impedances and fault currents between phase x and phase y, respectively.

Fault currents $\mathbf{I}^{\mathrm{f}}_{\mathrm{fault}}$ and $\mathbf{I}^{\mathrm{b}}_{\mathrm{fault}}$ are now included in the (12) and (13) to fully and correctly represent the faulty bus k and then read:

$$\begin{bmatrix}\Delta\mathbf{U}^{\mathrm{f}}_{\mathrm{k}}\\ \Delta\mathbf{I}^{\mathrm{f}}_{\mathrm{k}}\end{bmatrix} = \mathbf{\Pi}^{-1}_{\mathrm{k-1}}\cdot\begin{bmatrix}\Delta\mathbf{U}^{\mathrm{f}}_{\mathrm{k-1}}\\ \Delta\mathbf{I}^{\mathrm{f}}_{\mathrm{k-1}}\end{bmatrix} - \begin{bmatrix}0\\ \mathbf{Y}^{\mathrm{lat}}_{\mathrm{k}}\cdot\Delta\mathbf{U}^{\mathrm{f}}_{\mathrm{k}} + \mathbf{I}^{\mathrm{f}}_{\mathrm{fault}}\end{bmatrix}, \tag{20}$$

$$\begin{bmatrix}\Delta\mathbf{U}^{\mathrm{b}}_{\mathrm{k}}\\ \Delta\mathbf{I}^{\mathrm{b}}_{\mathrm{k}}\end{bmatrix} = \mathbf{\Pi}_{\mathrm{k}}\cdot\begin{bmatrix}\Delta\mathbf{U}^{\mathrm{b}}_{\mathrm{k+1}}\\ \Delta\mathbf{I}^{\mathrm{b}}_{\mathrm{k+1}}\end{bmatrix} + \begin{bmatrix}0\\ \mathbf{Y}^{\mathrm{lat}}_{\mathrm{k}}\cdot\Delta\mathbf{U}^{\mathrm{b}}_{\mathrm{k}} + \mathbf{I}^{\mathrm{b}}_{\mathrm{fault}}\end{bmatrix}. \tag{21}$$

Using (12) and (13) for buses without fault and (20) and (21) for a faulty bus k, we obtain a complete representation of the network. This means that the voltages in each of the buses should be the same regardless of the direction of computation, and consequently the voltage discrepancies between forward and backward computations should converge to zero. This knowledge can then be used to define an optimization problem with

the objective function to be minimized:

$$\sum_{i\in\{1,2,\ldots,n\}} |\Delta \mathbf{U}_i^f - \Delta \mathbf{U}_i^b|, \tag{22}$$

where n is the total number of MST buses. In other words, the objective function reaches its minimum when the GFM fault currents are correctly determined. From (18) and (19), it can be seen that the only unknowns in the calculation of the fault currents are the unknown impedances of the GFM. Thus, by taking the impedances $Z_{a\text{-}b}$, $Z_{b\text{-}c}$, $Z_{c\text{-}a}$, $Z_{a\text{-}g}$, $Z_{b\text{-}g}$ and $Z_{c\text{-}g}$ in Fig. 5 as optimization variables and minimizing the objective function (22), their values are determined directly. From the known values of fault impedances, the type of fault is also revealed.

At this point, it should be noted what happens if the fault occurs on the lateral that is not part of the MST. In this case, the GFM parameters are still calculated as if the fault was located in the previously determined MST bus, regardless of the fact that the actual fault location is somewhere on the lateral that stems from this bus. This in turn leads to overestimating the fault impedances by the value of the lateral impedance between the MST bus and the fault location. How we can efficiently exploit this fact is explained in the next subsection.

D. Extension of Fault Localization Beyond the Minimum Spanning Tree

With the methodology presented so far, we are able to determine the exact location of a fault, whether on the bus or somewhere on the line, for the MST. In this subsection, we extend fault localization beyond the MST without using additional PMUs at the end of laterals (without increasing the number of MST buses) in order to reduce implementation costs in the real environment. The idea is to use the calculated impedances from the previous subsection and the fact that short-circuit faults are purely resistive. Thus, if the calculated imaginary part (reactance) of the affected GFM impedance is close to zero, we can conclude that the fault location is actually on an MST. However, if the impedance also contains an imaginary part, the fault location must be on the lateral originating from the previously determined MST bus. This is a consequence of trying to model both the part of the network (between the actual fault location and an MST bus) and the fault itself using only a GFM. The fact that the lines themselves also have an inductive and capacitive component then reflects in the imaginary part of the calculated fault impedance not being zero. Therefore, by finding the position on the lateral where the absolute value of the fault reactance is lowest, one can determine the location of faults on laterals as well. Note that this extension is only applicable to short-circuit faults where we can assume that the impedance change is purely resistive. For power quality type of events such as capacitor bank switching, load switching or distributed energy source switching, which were also considered in [19], the same assumption cannot be made and an additional PMU is still required at the end of the lateral to locate such an event.

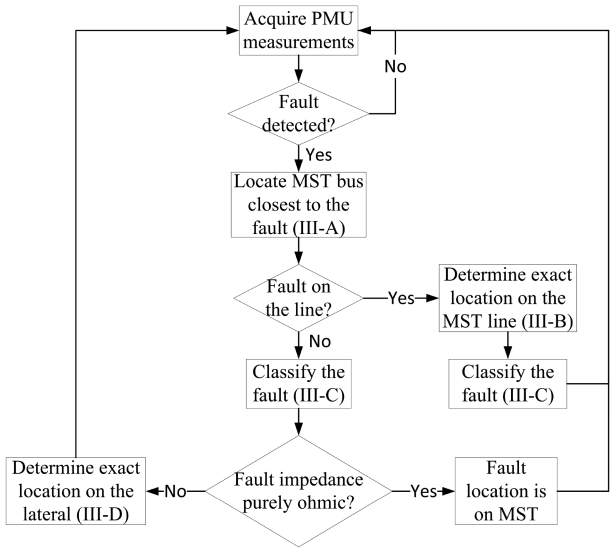

Fig. 6. Simplified flowchart of the proposed fault localization and classification method.

Using the concept of the virtual bus introduced in Section III-B, we can again calculate voltages and currents for any point along the lateral. However, since the PMU is not present at the end of the lateral, only the forward calculation, starting from the previously determined MST bus, is used. Once the voltages and currents on the lateral are known, the fault impedances at the new location can be easily determined using the (18) and (19). To avoid testing every single line of the lateral and to speed up the process, it is recommended to first assume that the fault location is in the physical buses of the lateral and calculate the corresponding fault impedances. Only when the reactance of the fault impedance changes sign from one bus to the other, the interconnecting line between them is tested in more detail using the virtual bus. Due to a numerical error, the reactance may not be exactly 0 in any of the buses. Therefore, we terminate the procedure and return the position of the fault on the lateral when the sign of the observed reactance changes in two consecutive virtual buses. It should be noted that the presented procedure no longer provides a unique solution when the lateral splits into two or more sublaterals, but returns a possible solution for each of them. Nevertheless, for the same number of PMUs, the presented novel use of the fault reactance still provides one level deeper insight into the network compared to existing methods.

E. Algorithm

The steps of the proposed method are shown in the flowchart in Fig 6. The PMU measurements are first checked for the presence of a fault. As mentioned earlier, this paper is only concerned with short-circuit faults, therefore, simple overcurrent and zero-sequence current detection methods are applied as fault detectors and necessary preliminary step for fault localization. Once the fault is detected, an MST bus closest to the fault location is determined using the equations of Section III-A. If the voltage discrepancy is above a certain threshold, all MST lines originating from this bus are checked as potential fault locations

using the refined fault localization procedure from Section III-B. Next, regardless of whether the fault is on one of the MST buses or anywhere on the MST line, the fault impedances are calculated using the optimization procedure from Section III-C. Finally, if the reactance of the fault in the determined MST bus is not close to zero, the lateral stemming from it is checked for a fault location using the procedure from Section III-D.

Note that the proposed method works under the following assumptions:

- synchronized phasors of voltages and currents before and during the fault are measured in at least two locations of the network;
- network topology, load/source locations and line parameters are available from the distribution system database;
- power profile at each bus is available as a pseudo-measurement (either through a demand/generation forecast, a state estimation method, or an actual smart meter (SM) measurement).

IV. Performance Evaluation and Comparative Study

The purpose of this section is twofold. First, it aims to verify the proposed fault localization and classification functions under ideal conditions, i.e., without uncertainties in the input parameters. Second, the precision of the proposed approach is compared with that of [19], which will be referred to as State of the Art (SotA) in the following. Note that faults occurring on the MST buses are excluded from the study, since in these cases the proposed method and SotA are essentially identical.

A. Simulation Environment and Power Network Specifics

In order to verify the proposed method, a simulation model of a distribution network was created in the Real Time Digital Simulator (RTDS) software environment RSCAD [25], which is specifically designed to solve electromagnetic transient (EMT) simulations in real time. RTDS is essentially a powerful computer whose processing units operate in parallel to achieve a continuous solution of the test model matrix equations with a time step of only 50 μs. In addition to the ability to simulate transient events such as faults, the RTDS provides software replicas of PMUs that faithfully mimic real PMUs by meeting the requirements of PMU standards for measurements [26] and communications [27]. Such simulations reproduce the operation of the method in the field and allow the creation of algorithm scripts that can be directly transferred from the test to the real environment. In our laboratory tests, the PMUs were configured to class P (protection) and reporting rate of 50 samples/s.

The topology of the 5.2 kV distribution network used to compare the effectiveness of the methods has already been shown in a single line diagram, Fig. 3. The model is based on a real three-phase, medium voltage (MV), low-impedance grounded distribution network, consisting of 16 buses and including both underground and overhead lines. Each of the lines is modelled with its own π-segment, while all loads are represented with constant impedances. The short-circuit level of the network is 54 MVA. In the simulations, the primary and secondary substations are monitored by PMUs, whereas each of the load buses is equipped with SM.

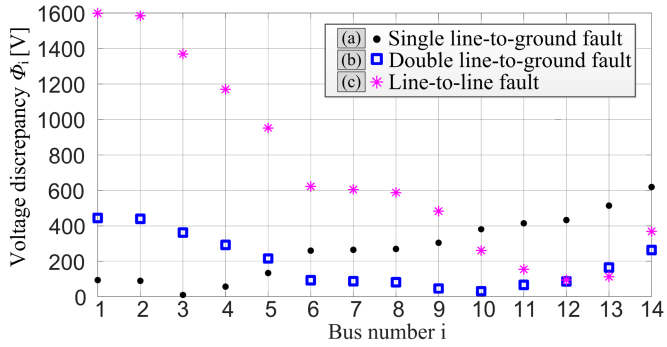

Fig. 7. Localization of a bus closest to fault using SotA - Section III-A.

Two sets of simulation tests are performed. The first set (presented in this section) is performed under ideal conditions and is designed to show the superior performance of the proposed method compared to SotA for any fault that occurs outside the MST buses. The second set (performed on a larger 48-bus network and presented in the next section) evaluates the accuracy of proposed method in a real environment where the input parameters are not 100% accurate, i.e., the performance of the method in the presence of errors in the power profiles, line parameters and measurements. In each set of tests, several cases are investigated considering different fault scenarios and fault impedances.

B. Evaluation of the Proposed Extension of Fault Localization Method on the Minimum Spanning Tree

In this part, it is assumed that the data collected in the field are free of errors. To demonstrate the effectiveness of the proposed extension of the fault localization method, three different types of faults were simulated in three different parts of the network. Fig. 7 shows the results of SotA for all three cases, where black dots denote the case of a single line-to-ground fault on 15% of the line length between buses 3 and 4, blue squares denote the case of a double line-to-ground fault on 60% of the line length between buses 9 and 10, and magenta asterisks denote the case of a line-to-line fault on 45% of the line length between buses 12 and 13. SotA correctly identifies bus 3 for the single line-to-ground fault, bus 10 for the double line-to-ground fault, and bus 12 for the line-to-line fault as the one closest to the fault, but, as mentioned earlier, it cannot determine the exact location of the fault on the line. For this reason, after determining the fault bus on MST, the voltage discrepancy in the lines to the adjacent buses is examined using the Section III-B step. The results of our approach for the same three cases are shown in the subplots of Fig. 8. In addition to the bus determined by SotA to be faulty and its neighbouring buses, the horizontal axes show the percentage of the line length connecting them. The results of SotA from Fig. 7 are shown here with red circles and the minimum value (solution) is marked with a black ring. On the other hand, the green line and ring are used to show the voltage discrepancy along the lines and the solution with the proposed method, respectively. The vertical dotted blue

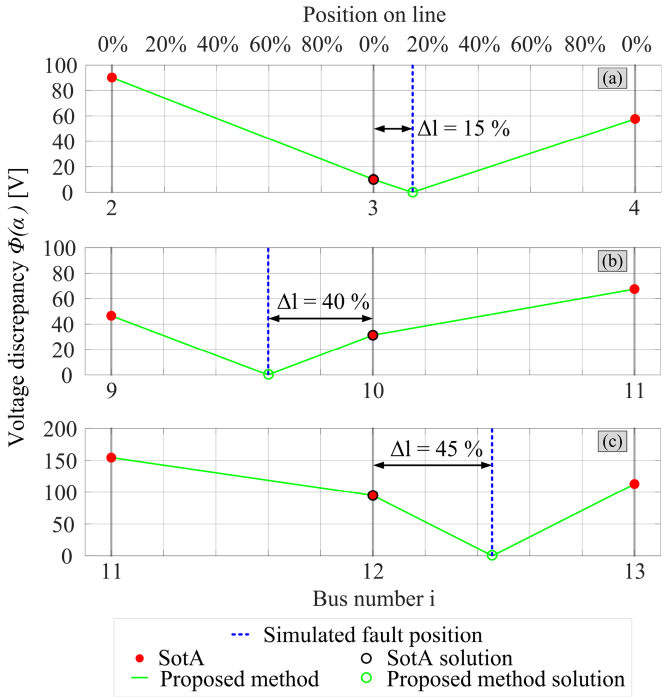

Fig. 8. Comparison of SotA and the proposed localization of the exact position on the line for (a) single line-to-ground fault, (b) double line-to-ground fault, (c) line-to-line fault.

TABLE II
CALCULATED FAULT IMPEDANCES FOR LINE-TO-GROUND FAULTS

Set fault impedance	Calculated fault impedance		
	$Z_{a\text{-}g}[\Omega]$	$Z_{b\text{-}g}[\Omega]$	$Z_{c\text{-}g}[\Omega]$
$R_{a\text{-}g} = 0.1\,\Omega$	0.0995	$2.25 \cdot 10^4$	$2.33 \cdot 10^4$
$R_{b\text{-}g} = 7.3\,\Omega$	$2.54 \cdot 10^4$	7.3004	$1.98 \cdot 10^4$
$R_{c\text{-}g} = 34\,\Omega$	$2.58 \cdot 10^4$	$1.94 \cdot 10^4$	34.0054
$R_{a\text{-}g} = 0.1\,\Omega$ $R_{b\text{-}g} = 7.3\,\Omega$	0.0996	7.3027	$2.28 \cdot 10^4$
$R_{a\text{-}g} = 0.1\,\Omega$ $R_{c\text{-}g} = 34\,\Omega$	0.0995	$2.22 \cdot 10^4$	34.0099
$R_{b\text{-}g} = 7.3\,\Omega$ $R_{c\text{-}g} = 34\,\Omega$	$2.55 \cdot 10^4$	7.3004	34.0060
$R_{a\text{-}g} = 0.1\,\Omega$ $R_{b\text{-}g} = 7.3\,\Omega$ $R_{c\text{-}g} = 34\,\Omega$	0.0996	7.3027	34.0100

line shows the simulated position of the line. It is clear that the minimum voltage discrepancy of proposed method matches the exact position of the fault in each of the cases and therefore outperforms SotA in terms of precision.

C. Evaluation of the Proposed Fault Classification Method

The proposed fault classification and fault impedance calculation functions are entirely new features added to SotA and are essential to our method of locating faults outside the MST. To verify their effectiveness, we simulated one of each common fault types and calculated the fault impedances of the introduced GFM according to Section III-C. The results of the line-to-ground faults are shown in Table II.

TABLE III
CALCULATED FAULT IMPEDANCES FOR LINE-TO-LINE FAULTS

Set fault impedance	Calculated fault impedance		
	$Z_{a\text{-}b}[\Omega]$	$Z_{b\text{-}c}[\Omega]$	$Z_{c\text{-}a}[\Omega]$
$R_{a\text{-}b} = 0.1\,\Omega$	0.0998	$6.92 \cdot 10^5$	$4.76 \cdot 10^5$
$R_{b\text{-}c} = 6.9\,\Omega$	$9.83 \cdot 10^{17}$	6.9006	$1.13 \cdot 10^{18}$
$R_{c\text{-}a} = 24.9\,\Omega$	$3.60 \cdot 10^4$	$3.72 \cdot 10^7$	24.9063
$R_{a\text{-}b} = 0.1\,\Omega$ $R_{b\text{-}c} = 6.9\,\Omega$	0.0998	6.9005	$4.76 \cdot 10^5$
$R_{a\text{-}b} = 0.1\,\Omega$ $R_{c\text{-}a} = 24.9\,\Omega$	0.0997	$5.79 \cdot 10^5$	24.9243
$R_{b\text{-}c} = 6.9\,\Omega$ $R_{c\text{-}a} = 24.9\,\Omega$	$7.91 \cdot 10^6$	6.8412	24.8537

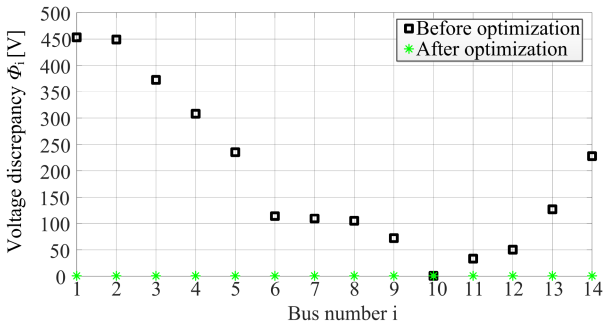

Fig. 9. Voltage discrepancy for a single line-to-ground fault in bus 10 before and after the optimization process.

The first column shows the impedances set in the simulation environment. As mentioned earlier, the short-circuit faults are purely resistive, so only the resistive component has been assigned. The following three columns show the GFM fault impedances, which are the result from the optimization process. We can observe a very good agreement between the assigned and the computed values for all cases. Moreover, the impedances of the GFM not involved in the fault have converged to very high values, which is also correct as this indicates that these phases are not involved in a fault. Since in the considered network faults with impedance values above ∼100 Ω no longer trigger the operation of the circuit breaker, we treat any calculated impedance above this threshold as not participating in the fault. From this, it is easy to classify the event as either a single, double, or triple line-to-ground fault.

Next, in Table III we present the results for line-to-line faults. Again, we find very good agreement between the set and calculated values, with the impedances of the GFM that are not involved in the faults being even higher compared to the line-to-ground faults.

Finally, we would like to highlight the fact that the voltage discrepancy Φ_i in each bus converges to 0 after the optimization process. In Fig. 9, the voltage discrepancy before the optimization process is shown with black squares and the voltage discrepancy after optimization is shown with green asterisks for a single phase-to-ground fault in bus 10. When the GFM is included in the faulted bus and the fault impedances are correctly

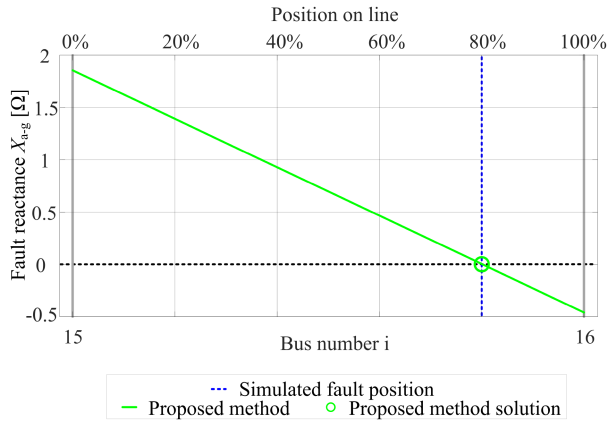

Fig. 10. Refined localization on the lateral using Section III-D for a single line-to-ground fault.

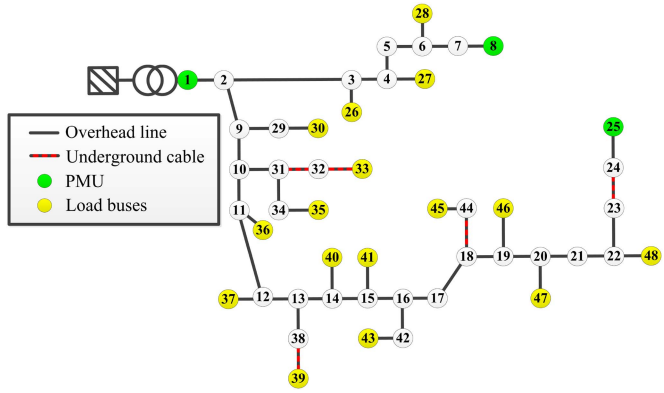

Fig. 11. Single-line diagram of 48-bus MV distribution network.

determined by the optimization process all voltage discrepancy values are indeed close to 0 as expected.

D. Evaluation of Fault Localization Beyond Minimum Spanning Tree

To demonstrate the effectiveness of the proposed method for the faults occurring outside the MST, we simulated a single line-to-ground fault on 80% of the line length between bus 15 and 16. Both SotA and step Section III-B of our method indicate MST bus 4 as the fault location. However, since step Section III-C shows that the reactance of the faulty phase would be $2.47\,\Omega$ if the fault was actually in this bus, we know that the fault must be located somewhere on the lateral instead. Therefore, we first assume the new fault location in buses 15 and 16 and obtain fault reactances of $1.85\,\Omega$ and $-0.46\,\Omega$, respectively. Since the fault reactance changes sign between buses 15 and 16, this line is examined in more detail using a virtual bus. Fig. 10 shows how the fault reactance changes when we change the assumed position of a fault on the line. It is clear that the fault reactance actually changes sign at about 80% of the line, which is again the correct fault location.

Note that since the SotA method would indicate bus 4 as faulty, the lines to buses 3 and 5, as well as the entire lateral 4–16, are potential fault candidates that would need to be physically checked. With the proposed extension, on the other hand, we can not only say that the fault is certainly on the lateral, but also calculate its exact location. In order for SotA to point to a bus 16 as the one closest to the fault, an additional PMU would have to be installed in bus 16, which in turn leads to higher implementation costs in the real environment. But even then, without the proposed Section III-B step, the exact localization on the line would not be possible with SotA.

V. Sensitivity Analysis

A. Power Network Specifics

To investigate the scalability of the method, a 48-bus MV network was used in the sensitivity analysis. The single-line diagram of this network, based on a real 35 kV distribution network with a short-circuit level of 1225 MVA, is shown in Fig. 11. Similar to the previous section, the lines are modelled as π-segments and the loads as constant impedances. The total length of the two feeders connecting the primary substation (bus 1) to the secondary substations (buses 25 and 8) are 21.1 km and 11.4 km, respectively. At this point, a brief discussion of the positioning of PMUs seems appropriate. You will recall from the methodology section that our method provides a unique solution for first-order laterals, i.e., laterals that do not split further into additional branches, otherwise we get a potential fault location on each of the sub-laterals. Unlike the 16-bus network used in Section IV, here it is impossible to cover the entire network with only two PMUs in such a way that all the laterals outside the MST are of first order. For example, using only the PMUs in buses 1 and 25, parts of network 3–4, 3–26, 31–33 and 31–35 would be considered second-order laterals, parts 4–6 and 4–27 would be third-order laterals and parts 6-8 and 6-28 would be fourth-order laterals. Two additional PMUs, e.g., in bus 8 and bus 33, completely eliminate the problem of higher-order laterals and allow our method to uniquely locate all faults. However, since feeders 31–33 and 31–35 (178 m and 85 m, respectively) are relatively short compared to feeders 1–25 and 1–8, the authors considered the use of only one additional PMU (in bus 8) sufficient for this particular case. In this way, we obtain two solutions only for the faults downstream of bus 31 (distance from this bus for each of the two sub-laterals), while all other faults can be localised to a unique location. The load buses and the locations of the PMUs used in the sensitivity analysis are marked with yellow and green circles, respectively, in Fig. 11.

B. Fault Localization Sensitivity Analysis

In this section, we investigate the robustness of the proposed fault localization improvements to certain ranges of uncertainty in the input parameters of the method. Recall that the method requires three types of input parameters, namely pseudo-measurements (power injections), grid model (line parameters) and PMU measurements of voltages and currents. For each of these parameters, four scenarios with different levels of error are performed using the Monte Carlo approach consisting of 10000 simulations. Then, the fault localization percentage error e is

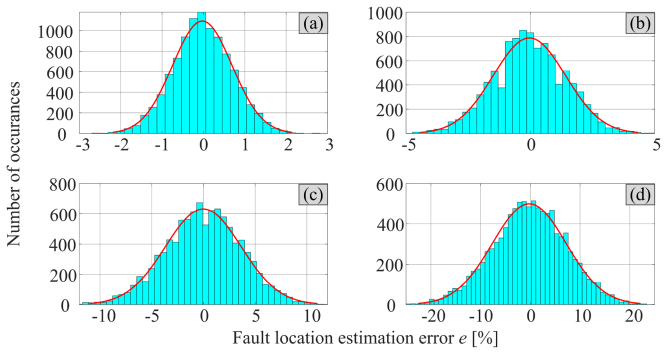

Fig. 12. Fault location estimation error e for scenarios with error in estimated power injection (a) scenario with 10% SD, (b) scenario with 20% SD, (c) scenario with 50% SD, (d) scenario with 100% SD.

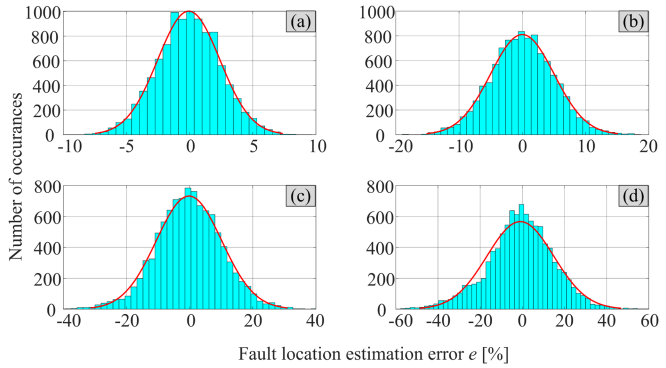

Fig. 13. Fault location estimation error e for scenarios with error in line parameters (a) scenario with 5% SD, (b) scenario with 10% SD, (c) scenario with 20% SD, (d) scenario with 30% SD.

calculated using the (23)

$$e = \frac{x_{\text{est}} - x_{\text{act}}}{l} \cdot 100\%, \tag{23}$$

where x_{est} and x_{act} are the estimated and actual fault location on the line and l is the total length of a faulty line. Finally, the histogram is plotted for each scenario. A red line in each scenario represents the probability density function corresponding to the mean value and standard deviation (SD) σ of the percentage error in estimating the fault location for that scenario.

Fig. 12 shows the results when errors occur in the estimation of the power injected into the buses. Scenarios for errors with 10%, 20%, 50% and 100% SD are considered. Note that these numbers are highly exaggerated when loads are monitored by SMs. However, we wanted to ensure that the method works adequately in cases where the power injection is estimated by a state estimation or demand/generation forecasting, which typically have a higher degree of error. We see that even for error with 100% SD in the injected power, fairly good results are obtained for the fault location estimation error (σ of probability density function is 7.41%).

Since the system operator's knowledge of the line parameters is imperfect, we next consider errors in these parameters with 5%, 10%, 20%, and 30% SD. The results for these scenarios are shown in Fig. 13. We used the error with 30% SD as the upper boundary condition, since it was argued in [19] that the impedance error with 25% SD is already beyond any normal level of error in practice. We see that errors in the line parameters affect the method much more than errors in the injected powers, but again, even for the worst scenario, the results show satisfying performance; σ of the fault location estimation error in that scenario is 15.84%.

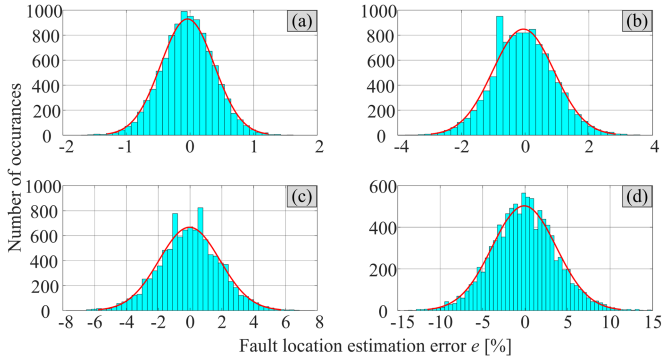

Fig. 14. Fault location estimation error e for scenarios with error in PMU measurements (a) 0.01% SD in amplitude, 0.003° SD in angle, (b) 0.025% SD in amplitude, 0.006° SD in angle, (c) 0.05% SD in amplitude, 0.01° SD in angle, (d) 0.1% SD in amplitude, 0.02° SD in angle.

Finally, we consider the impact of PMU measurements error on method performance. Note that PMUs capture and stream synchrophasors, which are basically vectors consisting of two parts (amplitude and angle). In this paper, we consider scenarios with combined percentage amplitude and absolute angle errors, which we adopted from [19]: a scenario with 0.01% amplitude and 0.003° angle error, a scenario with 0.025% amplitude and 0.006° angle error, a scenario with 0.05% amplitude and 0.01° angle error, and a scenario with 0.1% amplitude and 0.02° angle error. In Fig. 14, we see that the above measurement errors do not significantly affect localization of faults; in the worst scenario σ of the fault location estimation error is 3.78%.

C. Fault Classification Sensitivity Analysis

To investigate the robustness of the proposed fault classification method to uncertainties in the input parameters, we ran 10000 Monte Carlo simulations for each of the possible fault types. Due to space constraints, only the results for the single line-to-ground, double line-to-ground and line-to-line faults are presented in the paper. Also, simultaneous errors of the parameters were considered, with 50% SD in the power injection, 10% SD in the line parameters, 0.1% SD in the PMU amplitude, and 0.02° SD in the PMU angle.

First, a single line-to-ground fault with $Z_{\text{a-g}} = 0.1\,\Omega$ is considered. Fig. 15(a) shows the distribution of the calculated values $Z_{\text{a-g}}$. We see that for this fault, the impedance of the faulted phase is calculated with extreme precision in all simulated cases; the mean of the calculated values is $0.1\,\Omega$ with SD of $7.73 \cdot 10^{-4}\,\Omega$. However, in some cases, the introduced errors in the input parameters affect the method in a way that leads to incorrect impedance calculation of the other two non-faulted phases. As a result, the fault is incorrectly identified as a double line-to-ground fault in 4.79% of the cases, and as a triple line-to-ground fault in 7.09% of the cases. Nevertheless, the misidentified impedances in these

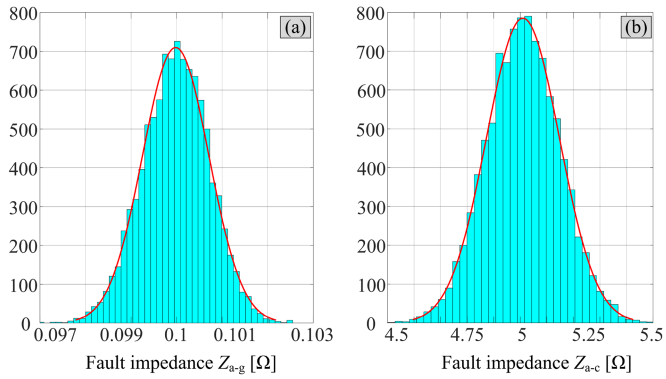

Fig. 15. Fault impedance obtained from optimization for (a) line-to-ground fault, (b) line-to-line fault.

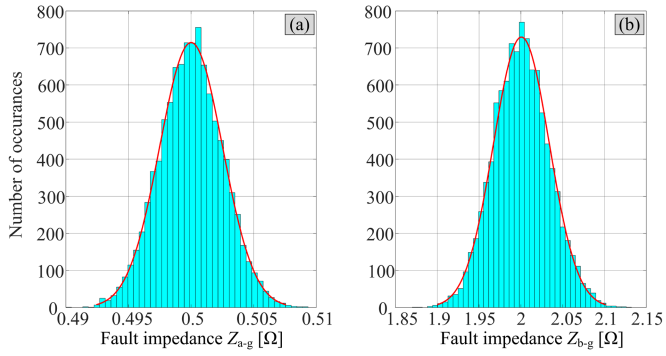

Fig. 16. Fault impedances of double line-to-ground fault obtained from optimization for (a) $Z_{a\text{-}g}$, (b) $Z_{b\text{-}g}$.

cases are calculated to be at least an order of magnitude higher than the true fault impedance.

Next, a line-to-line fault, with fault impedance $Z_{a\text{-}c} = 5\,\Omega$ is considered. In all simulated cases, the method correctly identifies the fault between phases a and c. Fig. 15(b) shows the distribution of the calculated values for the fault impedance, which has a mean value $5.01\,\Omega$ and SD of $0.1378\,\Omega$. In this scenario, the performance of the classification is better than in the previous scenario, as only 1.46% of the cases are incorrectly identified as three-phase faults.

Finally, we consider a double line-to-ground fault, with fault impedances $Z_{a\text{-}g} = 0.5\,\Omega$ and $Z_{b\text{-}g} = 2\,\Omega$. Fig. 16 shows the distribution of calculated values for both impedances. Also in this scenario, we see that the two faulted phases are correctly identified as faulted in all simulated cases, with very satisfactory values for impedances; the mean value of $Z_{a\text{-}g}$ is $0.5\,\Omega$ with SD of $0.0251\,\Omega$ and the mean value of $Z_{b\text{-}g}$ is $2.001\,\Omega$ with SD of $0.0334\,\Omega$. However, due to introduced errors in input parameters the third, non-faulted phase is also identified as faulted in 11.21% of the cases.

D. Computation Time

Knowing the computation speed is another metric of interest when evaluating fault localization algorithms. The computation time is affected by many factors, such as the size of the network, the programming language, the optimization technique, the available computational power, etc. The proposed method was implemented on a HP ZBook 15 G5 with an i7 2.2 GHz CPU, 16 GB RAM and running Windows 10. The entire workflow of the method, from reading and parsing the PMU data streams to the final fault classification, as shown in Fig. 6, is implemented in Python 3.9. The optimization problem of Section III-C is solved using the Powell method of the SciPy optimization library [28].

The total time of the method consists of three parts, namely the time to locate the MST bus closest to the bus, the time to locate the exact position on the line, and the time to classify the fault. For the network presented here, the typical values are 3.9 ms, 0.29 s, and 1.32 s, respectively. With a total time for fault localization and classification of less than 2 s, the proposed method can be considered as near real-time.

VI. Conclusion

In this paper, a fault localization and classification algorithm based on PMU measurements for power distribution systems is developed. A concept of a virtual bus on the line is presented, which allows more accurate fault localization in cases where the fault occurs on an arbitrary point on a line between two buses. In addition, the fault localization functionality is intuitively extended to include fault impedance calculation and fault classification. This is achieved by introducing a generic fault model at the previously determined fault location and solving the optimization problem. As the complex values of the fault impedances are determined, the location of faults occurring at the laterals outside the MST can also be determined by minimizing the fault reactance, thus eliminating the need for additional PMUs at the corresponding lateral ends. The newly introduced concepts are extensively tested on real-time digital simulator models of two real power distribution systems. The results show satisfactory performance and robustness of the proposed improvements to errors in measurements and input parameters.

References

[1] S. S. Gururajapathy, H. Mokhlis, and H. A. Illias, "Fault location and detection techniques in power distribution systems with distributed generation: A review," *Renewable Sustain. Energy Rev.*, vol. 74, pp. 949–958, 2017.

[2] A. Bahmanyar, S. Jamali, A. Estebsari, and E. Bompard, "A comparison framework for distribution system outage and fault location methods," *Electric Power Syst. Res.*, vol. 145, pp. 19–34, 2017.

[3] *IEEE Guide for Determining Fault Location on AC Transmission and Distribution Lines*, IEEE Std C37. 114-2014 (Revision of IEEE Std C37.114-2004), 2015.

[4] A. Borghetti, M. Bosetti, C. A. Nucci, M. Paolone, and A. Abur, "Integrated use of time-frequency wavelet decompositions for fault location in distribution networks: Theory and experimental validation," *IEEE Trans. Power Del.*, vol. 25, no. 4, pp. 3139–3146, Oct. 2010.

[5] J. Mora-Florez, J. Meléndez, and G. Carrillo-Caicedo, "Comparison of impedance based fault location methods for power distribution systems," *Electric Power Syst. Res.*, vol. 78, no. 4, pp. 657–666, 2008.

[6] M. Majidi, A. Arabali, and M. Etezadi-Amoli, "Fault location in distribution networks by compressive sensing," *IEEE Trans. Power Del.*, vol. 30, no. 4, pp. 1761–1769, Aug. 2015.

[7] M. Jamei et al., "Phasor measurement units optimal placement and performance limits for fault localization," *IEEE J. Sel. Areas Commun.*, vol. 38, no. 1, pp. 180–192, Jan. 2020.

[8] O. Ardakanian, Y. Yuan, R. Dobbe, A. von Meier, S. Low, and C. Tomlin, "Event detection and localization in distribution grids with phasor measurement units," in *Proc. IEEE Power Energy Soc. Gen. Meeting*, 2017, pp. 1–5.
[9] M. Biswal, S. M. Brahma, and H. Cao, "Supervisory protection and automated event diagnosis using PMU data," *IEEE Trans. Power Del.*, vol. 31, no. 4, pp. 1855–1863, Aug. 2016.
[10] F. Conte, F. D'Agostino, B. Gabriele, G.-P. Schiapparelli, and F. Silvestro, "Fault detection and localization in active distribution networks using optimally placed phasor measurements units," *IEEE Trans. Power Syst.*, vol. 38, no. 1, pp. 714–727, Jan. 2023.
[11] A. Ahmed, K. S. Sajan, A. Srivastava, and Y. Wu, "Anomaly detection, localization and classification using drifting synchrophasor data streams," *IEEE Trans. Smart Grid*, vol. 12, no. 4, pp. 3570–3580, Jul. 2021.
[12] M. Pignati, L. Zanni, P. Romano, R. Cherkaoui, and M. Paolone, "Fault detection and faulted line identification in active distribution networks using synchrophasors-based real-time state estimation," *IEEE Trans. Power Del.*, vol. 32, no. 1, pp. 381–392, Feb. 2017.
[13] W. Li, D. Deka, M. Chertkov, and M. Wang, "Real-time faulted line localization and PMU placement in power systems through convolutional neural networks," *IEEE Trans. Power Syst.*, vol. 34, no. 6, pp. 4640–4651, Nov. 2019.
[14] M. Gholami, A. Abbaspour, M. Moeini-Aghtaie, M. Fotuhi-Firuzabad, and M. Lehtonen, "Detecting the location of short-circuit faults in active distribution network using PMU-Based state estimation," *IEEE Trans. Smart Grid*, vol. 11, no. 2, pp. 1396–1406, Mar. 2020.
[15] R. A. F. Pereira, L. G. W. da Silva, M. Kezunovic, and J. R. S. Mantovani, "Improved fault location on distribution feeders based on matching during-fault voltage sags," *IEEE Trans. Power Del.*, vol. 24, no. 2, pp. 852–862, Apr. 2009.
[16] M. Majidi and M. Etezadi-Amoli, "A new fault location technique in smart distribution networks using synchronized/nonsynchronized measurements," *IEEE Trans. Power Del.*, vol. 33, no. 3, pp. 1358–1368, Jun. 2018.
[17] M. U. Usman and M. O. Faruque, "Validation of a PMU-based fault location identification method for smart distribution network with photovoltaics using real-time data," *IET Gener., Transmiss. Distrib.*, vol. 12, no. 21, pp. 5824–5833, 2018.
[18] G. Liu, H. Chen, X. Sun, N. Quan, L. Wan, and R. Chen, "Low-complexity nonlinear analysis of synchrophasor measurements for events detection and localization," *IEEE Access*, vol. 6, pp. 4982–4993, 2018.
[19] M. Farajollahi, A. Shahsavari, E. M. Stewart, and H. Mohsenian-Rad, "Locating the source of events in power distribution systems using Micro-PMU data," *IEEE Trans. Power Syst.*, vol. 33, no. 6, pp. 6343–6354, Nov. 2018.
[20] P. A. Cavalcante and M. C. de Almeida, "Fault location approach for distribution systems based on modern monitoring infrastructure," *IET Gener., Transmiss. Distrib.*, vol. 12, no. 1, pp. 94–103, 2018.
[21] Q. Cui and Y. Weng, "Enhance high impedance fault detection and location accuracy via μPMUs," *IEEE Trans. Smart Grid*, vol. 11, no. 1, pp. 797–809, Jan. 2020.
[22] A. Khaleghi, M. O. Sadegh, and M. G. Ahsaee, "Permanent fault location in distribution system using phasor measurement units (PMU) in phase domain," *Int. J. Elect. Comput. Eng.*, vol. 8, no. 5, 2018, Art. no. 2709.
[23] S. Lotfifard, M. Kezunovic, and M. J. Mousavi, "Voltage sag data utilization for distribution fault location," *IEEE Trans. Power Del.*, vol. 26, no. 2, pp. 1239–1246, Apr. 2011.
[24] R. Salim, K. Salim, and A. Bretas, "Further improvements on impedance-based fault location for power distribution systems," *IET Gener., Transmiss. Distrib.*, vol. 5, no. 4, pp. 467–478, 2011.
[25] RTDS Technologies, "RSCAD: Real-time simulation software package." Accessed: Sep. 2022. [Online]. Available: https://knowledge.rtds.com/hc/en-us/articles/360046352893-RSCAD-Real-Time-Simulation-Software-Package
[26] *IEEE/IEC International Standard - Measuring Relays and Protection Equipment - Part 118-1: Synchrophasor for Power Systems - Measurements*, IEC/IEEE 60255-118-1:2018, 2018.
[27] *IEEE Standard for Synchrophasor Data Transfer for Power Systems*, IEEE Std C37.118.2-2011 (Revision of IEEE Std C37.118-2005), 2011.
[28] "scipy.optimize.minimize - SciPy v1.7.1 manual." Accessed: Sep. 2022. [Online]. Available: https://docs.scipy.org/doc/scipy/reference/generated/scipy.optimize.minimize.html

Denis Sodin recieved the B.Sc. and M. Sc. degrees in electrical engineering from the University of Ljubljana, Ljubljana, Slovenia, in 2014 and 2017, respectively. Since graduation, he has been working with the Jožef Stefan Institute as a Research Assistant and at ComSensus as a Research and Innovation Engineer and domain Expert. His research interests include improvement of conventional under-frequency load shedding, applicability of PMU data for fault detection, localization and classification in power distribution networks, and hardware-in-the-loop testing with a real-time digital simulator.

Miha Smolnikar received the B.Sc. degree in electrical engineering from the University of Ljubljana, Ljubljana, Slovenia, in 2005. After graduation, he joined Jožef Stefan Institute as a Researcher with the Department of Communication Systems. In 2011, he co-founded a high-tech company ComSensus, developing digitalization solutions for various industries. He has more than 15 years of experience in embedded systems, wireless communications, and smart grids. He actively participates in EU funded collaborative projects and has published several peer-reviewed journal and conference papers.

Urban Rudež (Member, IEEE) received the B.Sc. and Ph.D. degrees from the University of Ljubljana, Ljubljana, Slovenia, in 2005 and 2011, respectively. After finishing his graduate study he worked with the Korona company, Ljubljana for two years as a system Engineer with the Department for Power Engineering. In 2007, he joined the Faculty of Electrical Engineering, Department of Power Systems and Devices, University of Ljubljana, where he still an Assistant Professor. His research interests include mostly power-system dynamic analysis. He is a Member of Cigre (Paris, France).

Andrej Čampa received the Ph.D. degree in electrical engineering from the University of Ljubljana, Ljubljana, Slovenia, in 2009, specializing in numerical methods and mathematical simulations. He has more than 10 years of experience working in R&D institutions covering diverse fields from photovoltaics, optoelectronics and semiconductor materials to numerical modeling and Big Data analytics, which represents his current expertise domain. His areas of interest at ComSensus and the Jožef Stefan Institute are closely related to understanding and optimization in smart grids.